

Breakdown of diffusion: From collisional hydrodynamics to a continuous quantum walk in a homogeneous Hubbard model

Ulrich Schneider,^{1,2,*} Lucia Hackermüller,¹ Jens Philipp Ronzheimer,^{1,2} Sebastian Will,^{1,2} Simon Braun,^{1,2} Thorsten Best,¹ Immanuel Bloch,^{1,2,3} Eugene Demler,⁴ Stephan Mandt,⁵ David Rasch,⁵ and Achim Rosch⁵

¹*Institut für Physik, Johannes Gutenberg-Universität, 55099 Mainz, Germany*

²*Fakultät für Physik, Ludwig-Maximilians-Universität, 80799 München, Germany*

³*Max-Planck-Institut für Quantenoptik, 85748 Garching, Germany*

⁴*Department of Physics, Harvard University, Cambridge, MA 02138, USA*

⁵*Institut für Theoretische Physik, Universität zu Köln, 50937 Cologne, Germany*

(Dated: May 21, 2010)

The law of diffusion governs the transport of heat and charge in most materials and has diverse applications ranging from the motion of cells to the pricing of stock options in financial markets. Here we investigate the breakdown of diffusion in the transport of fermionic quantum particles on a lattice described by a homogeneous Hubbard model. We observe a crossover from diffusive behaviour in the center of the cloud to a ballistic motion of atoms in its outer regions. This crossover manifests itself in a striking change of the cloud's shape: While it remains round in the diffusive regime, it obtains a square shape when the motion becomes ballistic. Surprisingly, the system exhibits a strong feedback from the ballistic on the diffusive regions characterized by a universal loss rate of particles obeying singular diffusion equations. In addition, the observed dynamics is independent of the sign of the interaction, highlighting a novel, dynamic symmetry of the Hubbard model.

The last years have seen dramatic progress in the control of quantum gases in optical lattices [1–3] using both bosonic and fermionic [4–10] gases as well as Bose-Fermi mixtures [11–13]. It has become possible to simulate models of strongly interacting quantum particles for which the Hubbard model [14] is probably the most important example. A major advantage of these systems compared to real solids is the possibility to change all relevant parameters in real-time by e.g. varying laser intensities or magnetic fields. This has led to several studies of dynamical properties of both bosonic [15–19] and fermionic quantum gases [8–10].

Fermionic atoms have been used to study the equilibrium phases of both the attractive [4] and repulsive Hubbard model [5–7] as well as dynamic properties of trapped systems [8–10]. One open, fundamental question in these experiments concerns the timescales needed to adiabatically load into the lattice [20–22] or to achieve equilibrium in the lattice [22, 23]. Up to now, all of these experiments were performed in the presence of additional potentials.

In this work, it was possible to eliminate all external potentials in a two-dimensional (2D) system by compensating the anticonfining potential of a blue-detuned optical lattice [6] and to study out-of-equilibrium dynamics and transport properties in a homogeneous Hubbard model.

To this end, an initially confined atomic cloud was allowed to expand freely within a homogeneous optical lattice (Fig. 1a) for various interactions. Monitoring the in-situ density distribution during the expansion allowed for several surprising experimental observations: Even

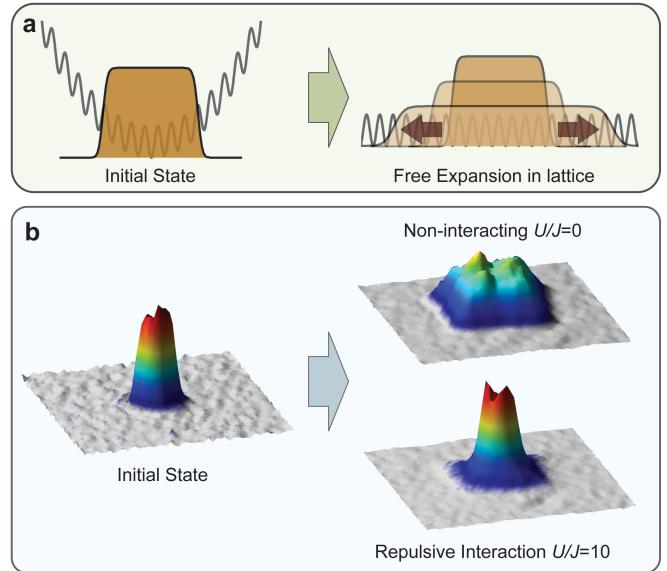


FIG. 1. **a**: Free expansion in a homogeneous lattice. First a band-insulator is created in the combination of an optical lattice and a strong harmonic trap. Subsequently the harmonic confinement is switched off and the cloud expands in a homogeneous Hubbard model. **b**: Observed in-situ density distributions. The evolution of the initial density distribution (left) crucially depends on the interaction (right).

small interactions (i) lead to a drastic reduction of the expansion velocity of the atomic cloud and (ii) change the shape of the expanding cloud. Despite the strong effects of the interactions, (iii) we never observe a \sqrt{t} dependence of the cloud size, which is expected for simple diffusive behaviour. (iv) For strong interactions the core width (see below) of the atomic cloud shrinks instead of expanding. And, finally, (v) we find that only the mag-

* ulrich.schneider@lmu.de

nitude but not the sign of the interaction matters: the dynamics is identical for repulsive and attractive interactions U .

In the non-interacting case the atoms expand ballistically in a continuous quantum walk [24–26], which is also the basis of a recently proposed quantum computing algorithm [27]. For long times, this ballistic expansion results in a square density distribution (see Fig. 1b) that reflects the lattice symmetry. Interactions between the atoms on the other hand lead to diffusive dynamics and allow the particles to regain local thermal equilibrium [28, 29]. As a consequence, sufficiently large atomic clouds, where density gradients are small, remain close to local thermal equilibrium and their dynamics can be described by the laws of hydrodynamics. Thereby the cloud retains its initial spherical symmetry (see Fig. 1b). In the outer regions of these clouds, however, the densities, and therefore the collision rates, become so small that also interacting atoms expand ballistically.

As diffusion in this system arises from collisions with other atoms, the time τ between scattering events and the diffusion constant $D \propto \tau$ are strongly density dependent and especially become very large when the density of particles n (or holes, $1 - n$) becomes very small, $D(n) \propto (n(1 - n))^{-1}$ (see Supplementary Information [30]). Accordingly, the dynamics is described by a highly singular, non-linear diffusion equation:

$$\partial_t n(r, t) = \nabla (D(n) \nabla n) \quad (1)$$

Such singular (or superfast) diffusion equations have been extensively studied in the mathematical literature [31] and show many surprising properties. For example, in three dimensions (3D), the diffusion equation (Eq. 1) predicts that all particles reach infinity in an infinitesimally short time, $n(r, t > 0) = 0$ if $D(n \rightarrow 0) \sim 1/n$ and if $\lim_{r \rightarrow \infty} n(r, t = 0) = 0$. This obviously unphysical result immediately implies the existence of a strong feedback from the ballistic onto the diffusive parts of the atomic cloud: The velocity limit imposed by the band structure on the ballistic outer regions constrains the maximal expansion velocity and thereby holds the diffusive part of the cloud together.

The situation is even more interesting in two dimensions (2D), where the non-linear diffusion equation predicts a *universal minimal loss rate* of the total number of particles N for $D(n) = \gamma/n$ [30–32]:

$$\partial_t N \leq -4\pi\gamma \quad (2)$$

This loss rate describes the rate of particles reaching infinity and is completely *independent* of the initial distribution. It only depends on boundary conditions at $r = \infty$, which can be chosen such that $\partial_t N = -4\pi\gamma$ [30–32]. We will show that this loss rate is closely related to the rate with which the diffusive part of the cloud emits ballistic particles.

Remarkably, the 2D diffusion equation and the universal loss rate have a very interesting geometrical interpretation [31]: Consider a curved manifold with a metric

$g_{ij} = n(\mathbf{r})\delta_{ij}$. In this case the diffusion equation for $D(n) = 1/n$ becomes equivalent to the famous Ricci flow $\frac{d}{dt}g_{ij} = -2R_{ij}$ [33, 34], which describes the evolution of a manifold that becomes flatter in time. Here R_{ij} is the Ricci tensor describing the curvature of the metric. Ricci flows play an important role in mathematics, especially for the proof of the celebrated Poincaré conjecture in three dimensions [34]. Within this interpretation, the particle loss rate is universal since $\partial_t N$ is proportional to the integral of the curvature over the manifold, which is a topological invariant [30].

I. EXPERIMENT

The experiment starts with the preparation of a quantum degenerate, balanced spin mixture of the two lowest hyperfine states $|F, m_F\rangle = |9/2, -9/2\rangle$ and $|9/2, -7/2\rangle$ of fermionic potassium ^{40}K in a crossed beam dipole trap [6]. Typical clouds consist of $N = 2\text{--}3 \times 10^5$ atoms at an initial temperature of $T/T_F = 0.13(2)$, where T_F denotes the Fermi temperature in the harmonic trap. Once cooled, the atoms are loaded into a three-dimensional blue-detuned optical lattice with lattice constant $\lambda/2 = 369\text{ nm}$, where their interaction is controlled by use of a Feshbach resonance at $B_0 = 202.1\text{ G}$ [35]. The employed loading procedure (see Supplementary Information [30]) results in a cloud of localized atoms with a well-known density distribution, which is independent of the interaction between the particles.

Subsequently, the expansion is initiated by switching off the harmonic confinement (see Fig. 1a). To this end, the strength of the dipole trap is reduced by more than 90%, such that for the horizontal directions the remaining dipole potential precisely compensates the anticonfinement produced by the lattice beams [30]. While the vertical motion is expected to be strongly suppressed by gravity-induced Bloch oscillations (Oscillation amplitude $2J/mg < 2\lambda/2$), the atoms are exposed to a homogeneous Hubbard model without additional potentials in the horizontal directions. The evolution of the density distribution during the following expansion in this *quasi* 2D situation was monitored by in-situ imaging along the vertical axis of the cloud, thereby integrating over any vertical dynamics. Absorption images of the resulting dynamics are shown in Fig. 2 for the case of non-interacting particles and in Fig. 4 for various interactions.

In a second set of experiments, vertical tunneling of the atoms during the expansion was suppressed by increasing the depth of the vertical lattice to $20 E_r$, with recoil energy $E_r = \hbar^2/(2m\lambda^2)$, thereby realizing several layers of independent two-dimensional Hubbard models without any influence of gravity.

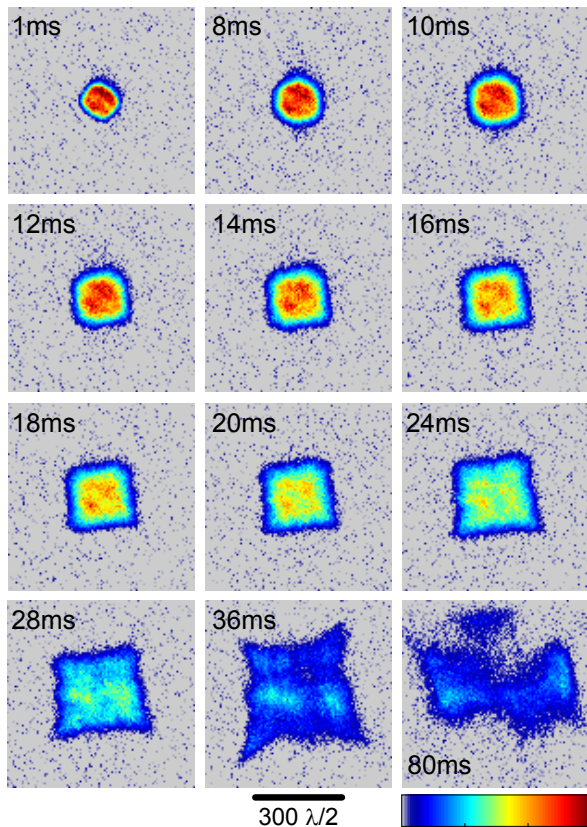


FIG. 2. In-situ absorption images (column density a.u.) of an expanding non-interacting cloud in a quasi 2D lattice with lattice depth $8E_r$. The expansion changes the symmetry of the cloud from the rotational symmetry of the harmonic trap to the square symmetry of the lattice Brillouin zone. At long expansion times residual potentials and lattice inhomogeneities deform the cloud (see Supplementary Information [30]).

II. NON-INTERACTING CASE

In the absence of collisions and additional potentials the Hubbard Hamiltonian (see Eq. A1 in [30]) consists only of the hopping term, which describes the tunneling of a particle from one lattice site to a neighbouring site with a rate J/\hbar . Each initially localized particle expands independently, and the density distribution after an evolution time t is given by the convolution of the initial density distribution with the delocalized probability distribution of the individual atoms. During the expansion the symmetry of the cloud changes from the rotational symmetry of the initial density distribution to a square symmetry that is governed by the symmetry of the lattice (Fig. 2). For very long expansion times, this symmetry becomes distorted by residual inhomogeneities in the remaining potential and in the lattice depth [30].

In order to extract the *mean expansion velocity* v_{exp} of the whole cloud we used Gaussian fits [30] to phase-contrast images and fitted the evolution of the resulting

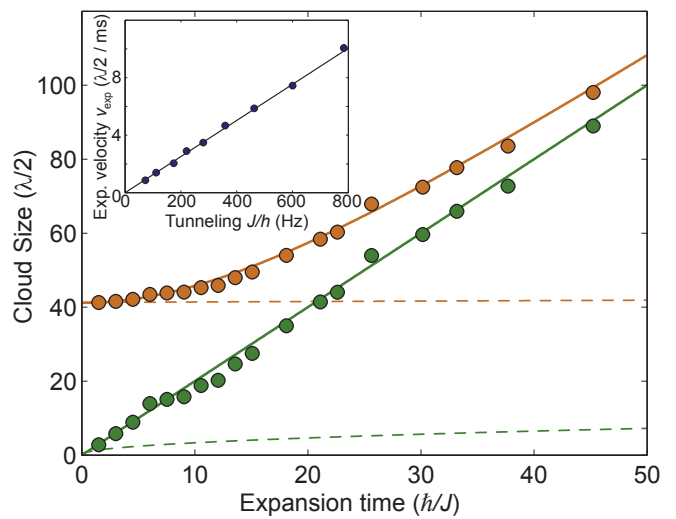


FIG. 3. Measured cloud size (orange) and deconvolved single-particle width (green) of an expanding non-interacting cloud in an $8E_r$ deep lattice. Solid lines denote the quantum-mechanical prediction and dashed lines the corresponding classical random walk. The inset shows the linear scaling of the mean expansion velocity with tunneling J .

cloud sizes (Fig. 3, orange) by

$$R(t) = \sqrt{R_0^2 + v_{\text{exp}}^2 t^2} \quad (3)$$

The deconvolved single-particle width $R_{\text{sp}} = \sqrt{R(t)^2 - R_0^2}$ (green) grows linearly in time, as expected for a ballistic expansion. In the classical case, thermal hopping of a particle (e.g. of a thermalized atom on the surface of a crystal) would result in a random walk, where at every timestep the particle randomly hops to *one* of the neighbouring sites. The width of the resulting density distribution scales as the square root of the expansion time. In the quantum case on the other hand, a particle tunnels in all directions simultaneously, which leads to a fundamentally different dynamics: The atoms expand ballistically with a mean squared velocity $v_{\text{exp}}^2 = \langle \mathbf{v}_{\mathbf{q}}^2 \rangle$, which is given by the mean squared group velocity $\mathbf{v}_{\mathbf{q}} = \frac{1}{\hbar} \frac{\partial E}{\partial \mathbf{q}}$ of all Bloch waves. Here $\hbar \mathbf{q}$ denotes the quasi-momentum and $E(\mathbf{q}) = -2J \sum_i \cos(q_i \frac{\lambda}{2})$ the dispersion relation in the lowest band. For particles that are initially localized to single lattice sites, the mean expansion velocity is $v_{\text{exp}} = \sqrt{2d} \frac{J}{\hbar} \frac{\lambda}{2}$ (d : dimension). As shown in Fig. 3, the experimentally observed ballistic expansion agrees well with the quantum-mechanical prediction (solid lines) while a classical random walk of the same hopping rate would predict a much slower square-root expansion of the single-particle width (dashed lines).

III. INTERACTING CASE

The ballistic expansion observed for non-interacting atoms is in stark contrast to the interacting case, where a qualitatively different dynamics is observed: Fig. 4 shows in-situ absorption images taken after 25 ms of quasi 2D expansion in an $8 E_r$ deep lattice.

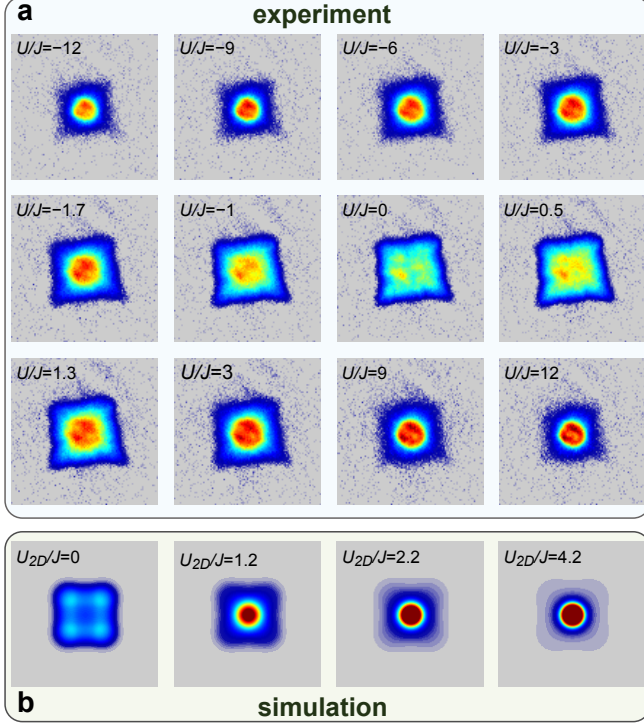


FIG. 4. In-situ absorption images for various interactions after 25 ms expansion in a homogeneous quasi 2D lattice. The images show a symmetric crossover from a ballistic expansion for non-interacting clouds to an interaction dominated expansion for both attractive and repulsive interactions. Images are averaged over at least five shots and all scales are identical to Fig. 2. The bottom line shows the results of a 2D simulation of the Boltzmann equation.

For increasing interaction strengths the center of the cloud expands much slower and preserves the initial rotational symmetry. The observed dynamics gradually changes from a purely ballistic expansion in the non-interacting case, which results in a square density distribution, into a more complex expansion for interacting atoms: In the center of the cloud frequent collisions guarantee the system to be close to local equilibrium [28–30] and the diffusion equation (Eq. 1) applies. As the diffusion equation is rotationally invariant, the initial spherical shape is preserved for most parts of the cloud already for moderately strong interactions, see Fig. 1 and 4. For a small fraction of atoms in the outer parts of the atomic cloud, however, the density is so small that scattering becomes rare, so that these atoms expand ballistically. Therefore the tails of the cloud show the square symme-

try characteristic for freely expanding particles (Fig. 4). This initial fraction of ballistically expanding atoms decreases for increasing interaction strengths. During the expansion the density gets reduced and, in the limit of infinite expansion times, all atoms are expected to become ballistic. We observe the same behaviour irrespective of the sign of the interactions.

The singular diffusion equation (Eq. 1) would predict diverging velocities for atoms at vanishing density. The ballistic part of the cloud, however, where the current $j \sim v_{exp} n$ is smaller than the current $-D(n)\nabla n$ predicted by the diffusion equation, obviously limits the spread of the diffusive parts of the cloud. This gives rise to a strong feedback from the ballistic tails on the diffuse core, as discussed in more detail in the Supplementary Information [30].

For a more quantitative analysis of our results, the same experiment was performed in a fully two-dimensional (2D) situation, where also numerical simulations are easier. In this experiment, the vertical lattice is kept at a depth of $20 E_r$ during the expansion in an otherwise identical sequence. In both cases (quasi 2D and 2D) one observes a spherical, diffusive core surrounded by ballistic tails without any qualitative differences between the cases.

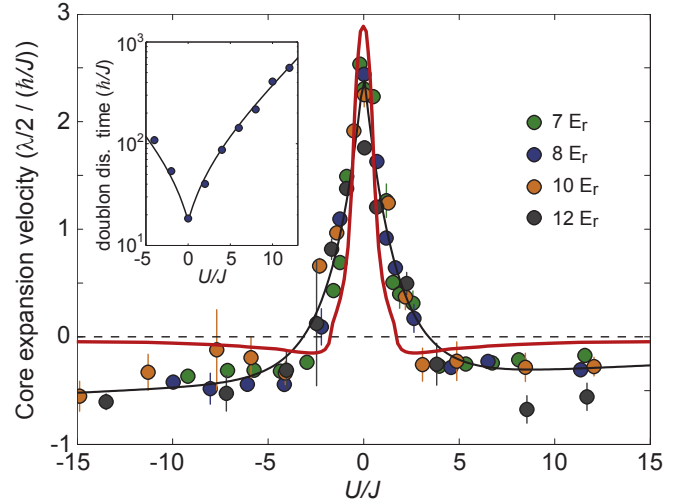


FIG. 5. Measured core expansion velocities versus interaction for various lattice depths in a 2D situation. The red line denotes the result of a numerical calculation (see text). The inset shows the doublon dissolution time (see Supplementary Information [30]) and both black lines are guides to the eye.

The core width $R_c(t)$, which measures the size of the high density core, is extracted from phase-contrast images by determining the half width at half maximum of the density distribution [30]. Surprisingly, the same simple fit function (Eq. 3) can still describe the time evolution (see Fig. 15 in [30]). The resulting core expansion velocities v_c , which are shown in Fig. 5, decrease dramatically already for interactions much smaller than the bandwidth $8J$. This highlights the strong impact of mod-

erate interactions on mass transport in these systems.

The core expansion velocities v_c even become negative for interactions larger than $|U/J| \gtrsim 3$: In this regime, the diffusive core dissolves by emitting ballistic particles and therefore shrinks in size. Solutions of the diffusion equation (Eq. 1) always show this behaviour for short and intermediate times, as the particle current in the flanks of the core is always higher than in the center of the core, where the density gradient vanishes. The slight asymmetry observed at large interactions can be attributed to interaction dependent losses due to light-assisted collisions during the preparation sequence.

This pronounced dependence on small interactions enabled us to measure the zero crossing of the scattering length ($B(a = 0) = 209.1 \pm 0.2$ G) and to extract a new calibration of the width of the Feshbach resonance: $w = 7.0 \pm 0.2$ G, see [30].

For a theoretical description of the expanding clouds one needs an approach that can correctly describe both the diffusive and the ballistic regime, the probably simplest one being the Boltzmann equation:

$$\partial_t f_{\mathbf{q}} + \mathbf{v}_{\mathbf{q}} \nabla_{\mathbf{r}} f_{\mathbf{q}} + \mathbf{F}(\mathbf{r}) \nabla_{\mathbf{q}} f_{\mathbf{q}} = -\frac{1}{\tau(\mathbf{n})} (f_{\mathbf{q}} - f_{\mathbf{q}}^0(\mathbf{n})) \quad (4)$$

It describes the evolution of the quasi-classical momentum distribution $f_{\mathbf{q}}(\mathbf{r}, t)$ as a function of position and time in the presence of a force \mathbf{F} (see [30] for details). Here the transport scattering time $1/\tau(\mathbf{n})$, which describes the relaxation towards an equilibrium distribution $f_{\mathbf{q}}^0$ for given energy (e) and particle densities (n) $\mathbf{n}(\mathbf{r}, t) = (n, e)$, is determined from a microscopic calculation of the diffusion constant for small interactions [30]. All qualitative features seen in the experiment are well reproduced by the numerical results using the Boltzmann equation. Fig. 5 shows that the numerical simulations describe the drastic collapse of the expansion velocities and the shrinking of the core width for strong interactions also semi-quantitatively. Quantitative discrepancies between experiment and numerics probably arise both because the leading order perturbation theory is not valid for $U \gtrsim J$ and because the relaxation time approximation breaks down in the crossover region from diffusive to ballistic behaviour, where the colliding atoms are far from thermal equilibrium [30].

Even though the core expansion velocity can be qualitatively predicted by a diffusive ansatz, the full quantum dynamics is certainly more complex and includes the formation of entanglement between distant atoms [36]. In the case of a sufficiently high initial doublon density the free expansion itself could possibly be used to locally cool the atoms via quantum distillation processes [37].

Our numerical results can be used to study the breakdown of the diffusion law (Eq. 1) and the role of the universal loss rate (Eq. 2). Fig. 6 shows that, for sufficiently strong interactions, the diffusion equation can describe the behaviour of the cloud center but breaks down in the tails. For a quantitative analysis of this effect we calculate the cloud size $\sqrt{\langle r^2 \rangle}$, which, in contrast to the

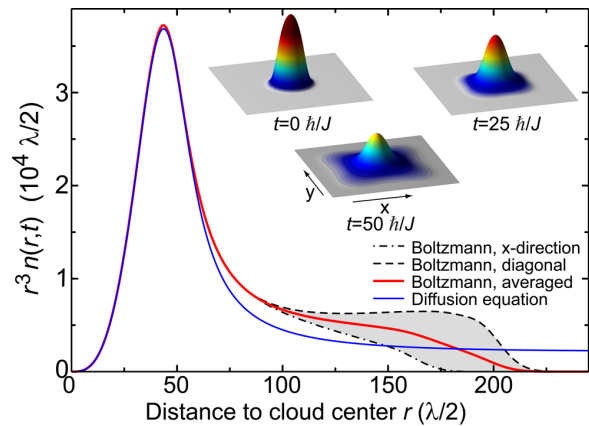


FIG. 6. Calculated density profile multiplied by r^3 from a simulation of the Boltzmann equation for $t = 50 \hbar/J$, $U = 4.15 J$. Dashed (dash-dotted) lines denote the density profiles along the diagonal (the x -direction). The diffusive center is rotationally invariant and is well described by the diffusion equation (blue line). In the ballistic tails, which have a large contribution to $\langle r^2 \rangle \propto \int n(r) r^3 dr$, the density profiles in diagonal and x -directions differ. The insets show density profiles of an expanding atomic cloud (consisting over several independent two-dimensional layers) for various expansion times and $U = 1.178 J$.

core width, is mostly sensitive to the ballistic parts of the cloud (see Fig. 6). Unfortunately, it cannot be reliably extracted from the experimental data due to a combination of a small signal-to-noise ratio in the extremely dilute regime and imaging aberrations. The universal loss rate suggests that ballistic particles, which are mainly responsible for the growth of the cloud size, are created at a constant rate. This implies that $\sqrt{\langle r^2 \rangle}$ grows as $t^{3/2}$ [30], as confirmed by the numerical simulations (see Fig. 10 in [30]). Furthermore, even the proportionality constant can be obtained analytically to within 20 % from the universal loss rate of Eq. 2. These numerical and analytical results strongly support the above picture of an emission rate of ballistic particles that is determined by the universal loss rate.

Both for the qualitative and quantitative analysis of our results, we assume the relaxation of the system to local equilibrium. For very strong attractive or repulsive interactions $|U| \gg J$, however, doubly occupied sites (doublons) only decay very slowly [23, 38, 39] as the missing or excess energy of order U cannot easily be transferred to other particles. An important question is whether the rate with which the diffusive core melts is determined by the decay time of *individual* doublons or whether the latter is fast compared to the former. The experimentally observed doublon dissolution times (Fig. 5) are about an order of magnitude larger than the decay time of excess doublons measured recently in a half filled situation [23] in 3D at comparable interactions. Furthermore, they match very well the typical timescales for melting of the diffusive core of the cloud observed within our simulations. We therefore conclude that for

the parameters used in our experiment the doubly occupied sites remain in local equilibrium in the diffusive regime.

Surprisingly, we measure identical density profiles and expansion rates for repulsive and attractive interactions of the same strength (see Fig. 5 and 4), although one would expect that repulsive (attractive) interactions lead to a positive (negative) pressure and therefore an increased (reduced) expansion rate. While this simple picture indeed applies for atoms with a quadratic dispersion $p^2/2m$, it is not correct for the Hubbard model with a periodic dispersion relation $E(\mathbf{q})$. In combination with an initial state that consists of a homogeneously filled Brillouin zone, where quasi-momenta with positive effective mass ($\partial^2 E(q)/\partial q^2 > 0$) and negative mass (hole-like states) are equally occupied, the high symmetry of the kinetic energy guarantees identical density profiles for interactions U and $-U$: As both initial state (localized atoms) and observable (density) are invariant under time reversal symmetry, the density dynamics is unchanged by the transformation $H \rightarrow -H$. In addition, they also remain invariant under a boost $\mathbf{q} \rightarrow \mathbf{q} + (\pi, \pi, \pi) \times \frac{2}{\lambda}$, which changes the sign of the hopping $J \rightarrow -J$. In combination, these two invariances give rise to the observed dynamical symmetry (see also [30]).

IV. CONCLUSION

Ultracold fermions in optical lattices offer many novel possibilities to study non-equilibrium dynamics as they allow for a full real-time control of most relevant parameters. Particularly they can implement so-called quantum quenches, where the Hamiltonian of the system is changed instantaneously. We studied the expansion of a cloud of initially localized atoms in a homogeneous Hubbard model and observed the crossover from a ballistic expansion at small densities or vanishing interactions to

hydrodynamic expansion in the interacting case. The feedback between the diffusive and ballistic parts of the cloud controls the expansion: the diffusive core slowly emits ballistic particles which in turn hold the diffusive part of the cloud together and regularize the otherwise singular diffusion in the tails. We observed identical behaviour for both attractive and repulsive interactions, highlighting the high symmetry of the kinetic energy in the Hubbard model.

The surprisingly large timescales of mass transport in an interacting Hubbard model set lower limits on the timescales needed both to adiabatically load the atoms into the lattice and to cool the system in the lattice [40]. They are therefore of paramount importance for all attempts to create complex, strongly correlated many-body states like Néel-ordered states in these systems. The method of directly measuring the expansion velocity can be generalized in a straightforward way to more complex quantum states including metallic and Mott-insulating states in the repulsive Hubbard model [6] or the pseudogap regime in the attractive Hubbard model [4]. In addition, the effects of various disorder potentials on the two-dimensional dynamics can be studied.

We thank Maria Moreno-Cardoner (LMU), Fabian Heidrich-Meisner (RWTH Aachen), David Pekker and Rajdeep Sensarma (Harvard), Bernd Kawohl, Claus Kiefer, Joachim Krug and Martin Zirnbauer (Cologne) for stimulating and insightful discussions.

This work was supported by the Deutsche Forschungsgemeinschaft (FOR801, SFB TR 12, SFB 608, Gottfried Wilhelm Leibniz Prize), the European Union (Integrated Project SCALA), EuroQUAM (L.H.), the US Defense Advanced Research Projects Agency (Optical Lattice Emulator program), the US Air Force Office of Scientific Research (Quantum Simulation MURI (E.D.)), the National Science Foundation (DMR-07-05472) (E.D.), the Harvard-MIT CUA (E.D.), MATCOR (S.W.) and the Gutenberg Akademie (S.W.).

-
- [1] D. Jaksch and P. Zoller, *Annals of Physics*, **315**, 52 (2005), ISSN 0003-4916, special Issue.
 - [2] M. Lewenstein, A. Sanpera, V. Ahufinger, B. Damski, A. Sen, and U. Sen, *Advances in Physics*, **56**, 243 (2007).
 - [3] I. Bloch, J. Dalibard, and W. Zwerger, *Rev. Mod. Phys.*, **80**, 885 (2008).
 - [4] L. Hackermüller, U. Schneider, M. Moreno-Cardoner, T. Kitagawa, T. Best, S. Will, E. Demler, E. Altman, I. Bloch, and B. Paredes, *Science*, **327**, 1621 (2010).
 - [5] R. Jördens, N. Strohmaier, K. Günter, H. Moritz, and T. Esslinger, *Nature*, **455**, 204 (2008).
 - [6] U. Schneider, L. Hackermüller, S. Will, T. Best, I. Bloch, T. A. Costi, R. W. Helmes, D. Rasch, and A. Rosch, *Science*, **322**, 1520 (2008).
 - [7] M. Köhl, H. Moritz, T. Stöferle, K. Günter, and T. Esslinger, *Phys. Rev. Lett.*, **94**, 080403 (2005).
 - [8] L. Pezzè, L. Pitaevskii, A. Smerzi, S. Stringari, G. Modugno, E. de Mirandes, F. Ferlaino, H. Ott, G. Roati, and M. Inguscio, *Phys. Rev. Lett.*, **93**, 120401 (2004).
 - [9] H. Ott, E. de Mirandes, F. Ferlaino, G. Roati, G. Modugno, and M. Inguscio, *Phys. Rev. Lett.*, **92**, 160601 (2004).
 - [10] N. Strohmaier, Y. Takasu, K. Günter, R. Jördens, M. Köhl, H. Moritz, and T. Esslinger, *Phys. Rev. Lett.*, **99**, 220601 (2007).
 - [11] K. Günter, T. Stöferle, H. Moritz, M. Köhl, and T. Esslinger, *Phys. Rev. Lett.*, **96**, 180402 (2006).
 - [12] S. Ospelkaus, C. Ospelkaus, O. Wille, M. Succo, P. Ernst, K. Sengstock, and K. Bongs, *Phys. Rev. Lett.*, **96**, 180403 (2006).
 - [13] T. Best, S. Will, U. Schneider, L. Hackermüller, D. van Oosten, I. Bloch, and D.-S. Lühmann, *Phys. Rev. Lett.*, **102**, 030408 (2009).
 - [14] J. Hubbard, *Proceedings of the Royal Society of London. Series A, Mathematical and Physical Sciences*, **276**, 238 (1963), ISSN 00804630.

- [15] H. Lignier, C. Sias, D. Ciampini, Y. Singh, A. Zenesini, O. Morsch, and E. Arimondo, *Phys. Rev. Lett.*, **99**, 220403 (2007).
- [16] M. Ben Dahan, E. Peik, J. Reichel, Y. Castin, and C. Salomon, *Phys. Rev. Lett.*, **76**, 4508 (1996).
- [17] C. D. Fertig, K. M. O'Hara, J. H. Huckans, S. L. Rolston, W. D. Phillips, and J. V. Porto, *Phys. Rev. Lett.*, **94**, 120403 (2005).
- [18] M. Gustavsson, E. Haller, M. J. Mark, J. G. Danzl, G. Rojas-Kopeinig, and H.-C. Nägerl, *Phys. Rev. Lett.*, **100**, 080404 (2008).
- [19] M. Fattori, C. D'Errico, G. Roati, M. Zaccanti, M. Jonas-Lasinio, M. Modugno, M. Inguscio, and G. Modugno, *Phys. Rev. Lett.*, **100**, 080405 (2008).
- [20] T. Gericke, F. Gerbier, A. Widera, S. Foelling, O. Mandel, and I. Bloch, *J. Mod. Opt.*, **54**, 735 (2007).
- [21] J. Wernsdorfer, M. Snoek, and W. Hofstetter, *Phys. Rev. A*, **81**, 043620 (2010).
- [22] C.-L. Hung, X. Zhang, N. Gemelke, and C. Chin, (2009), [arXiv.org:0910.1382](https://arxiv.org/abs/0910.1382).
- [23] N. Strohmaier, D. Greif, R. Jördens, L. Tarruell, H. Moritz, T. Esslinger, R. Sensarma, D. Pekker, E. Altman, and E. Demler, *Phys. Rev. Lett.*, **104**, 080401 (2010).
- [24] Y. Aharonov, L. Davidovich, and N. Zagury, *Phys. Rev. A*, **48**, 1687 (1993).
- [25] E. Farhi and S. Gutmann, *Phys. Rev. A*, **58**, 915 (1998).
- [26] M. Karski, L. Forster, J.-M. Choi, A. Steffen, W. Alt, D. Meschede, and A. Widera, *Science*, **325**, 174 (2009).
- [27] A. M. Childs, R. Cleve, E. Deotto, E. Farhi, S. Gutmann, and D. A. Spielman, in *STOC '03: Proceedings of the thirty-fifth annual ACM symposium on Theory of computing* (ACM, New York, NY, USA, 2003) pp. 59–68, ISBN 1-58113-674-9.
- [28] M. Rigol, V. Dunjko, and M. Olshanii, *Nature*, **452**, 854 (2008).
- [29] M. Eckstein, M. Kollar, and P. Werner, *Phys. Rev. Lett.*, **103**, 056403 (2009).
- [30] “See Supplementary Information.”
- [31] J. L. Vázquez, *Smoothing and Decay Estimates for Non-linear Diffusion Equations* (Oxford University Press, Oxford, 2006).
- [32] P. Daskalopoulos and M. A. Del Pino, *Comm. Analysis and Geometry*, **3**, 523 (1995).
- [33] R. S. Hamilton, *Contemporary Math.*, **71**, 237 (1988).
- [34] G. Perelman, [arXiv:math/0307245](https://arxiv.org/abs/math/0307245) (2003).
- [35] T. Loftus, C. A. Regal, C. Ticknor, J. L. Bohn, and D. S. Jin, *Phys. Rev. Lett.*, **88**, 173201 (2002).
- [36] O. Romero-Isart, K. Eckert, C. Rodo, and A. Sanpera, *J. Phys. A*, **40**, 8019 (2007).
- [37] F. Heidrich-Meisner, S. R. Manmana, M. Rigol, A. Muramatsu, A. E. Feiguin, and E. Dagotto, *Phys. Rev. A*, **80**, 041603 (2009).
- [38] K. Winkler, G. Thalhammer, F. Lang, R. Grimm, J. Hecker Denschlag, A. Daley, A. Kantian, H. Büchler, and P. Zoller, *Nature*, **441**, 853 (2006).
- [39] A. Rosch, D. Rasch, B. Binz, and M. Vojta, *Phys. Rev. Lett.*, **101**, 265301 (2008).
- [40] J.-S. Bernier, C. Kollath, A. Georges, L. De Leo, F. Gerbier, C. Salomon, and M. Köhl, *Phys. Rev. A*, **79**, 061601 (2009).
- [41] S. Will, T. Best, U. Schneider, L. Hackermüller, D.-S. Lühmann, and I. Bloch, *Nature*, **465**, 197 (2010).
- [42] P. Rosenau, *Phys. Rev. Lett.*, **74**, 1056 (1995).
- [43] I. T. Pedron, R. S. Mendes, T. J. Buratta, L. C. Malacarne, and E. K. Lenzi, *Phys. Rev. E*, **72**, 031106 (2005).
- [44] T. Kamimura and J. M. Dawson, *Phys. Rev. Lett.*, **36**, 313 (1976).
- [45] F. Helfferich and M. S. Plesset, *J. Chem. Phys.*, **28**, 418 (1958).
- [46] J. Lopez, C. A. Miller, and E. Ruckenstein, *J. Colloid Interface Sci.*, **56**, 460 (1976).
- [47] D. Bonn, J. Eggers, J. Indekeu, J. Meunier, and E. Rolley, *Rev. Mod. Phys.*, **81**, 739 (2009).
- [48] G. Barenblatt, *Akad. Nauk SSSR. Prikl. Mat. Meh.*, **16**, 679 (1952).
- [49] J. L. Vázquez, *Journal Math. Pures et Appliquées*, **71**, 503 (1992).
- [50] J. M. Ziman, *Electrons and Phonons* (Oxford University Press, New York, 1960).
- [51] S. Kim, *Group theoretical methods* (Cambridge University Press, Cambridge, 1999).
- [52] A. Sorensen, E. Altman, M. Gullans, J. V. Porto, M. D. Lukin, and E. Demler, “Adiabatic preparation of many-body states in optical lattices,” (2009), [arXiv.org:0906.2567](https://arxiv.org/abs/0906.2567).
- [53] J. J. García-Ripoll, M. A. Martin-Delgado, and J. I. Cirac, *Phys. Rev. Lett.*, **93**, 250405 (2004).

Appendix A: Supplementary Information

1. Experimental sequence

The experiment starts with the preparation of a band-insulating state of a balanced spin mixture of fermionic potassium ^{40}K , as described in previous work [6]: Through evaporative cooling in a red-detuned crossed dipole trap a quantum degenerate mixture of the two lowest hyperfine states of potassium was reached with atom numbers of $N = 1 - 1.5 \times 10^5$ atoms per spin state at a temperature of $T/T_F = 0.13(2)$, where T_F denotes the Fermi temperature in the harmonic trap. The trapping frequencies of the dipole trap were then increased to $2\pi \times 100 \text{ Hz}$ ($2\pi \times 400 \text{ Hz}$) in the horizontal (vertical) directions.

Subsequently, a simple-cubic blue-detuned 3D optical lattice ($\lambda = 738 \text{ nm}$) is ramped up linearly to a depth of $8E_r$ ($1E_r = \hbar^2/(2m\lambda^2)$) in 56 ms while the magnetic field is held at 209.1 G, which corresponds to vanishing interactions (see A 6). This loading procedure results in a band-insulating state surrounded by a thin metallic shell at a compression of $E_t/12J = 1.8$, using units and conventions of Ref. [6]. In the next step, the tunneling rate J is reduced to $J = \hbar \times 23 \text{ Hz}$ by linearly increasing the lattice depth to $20E_r$ in $200 \mu\text{s}$, a timescale that is slow enough to avoid excitations into excited bands, but fast compared to tunneling within the lowest band. Due to this reduced tunneling rate the density distribution is essentially frozen out during the following 40 ms magnetic field ramp ($B_{dyn} = 206 - 260 \text{ G}$), which sets the interaction for the expansion. Combined with the strong harmonic confinement, this leads to a dephasing between

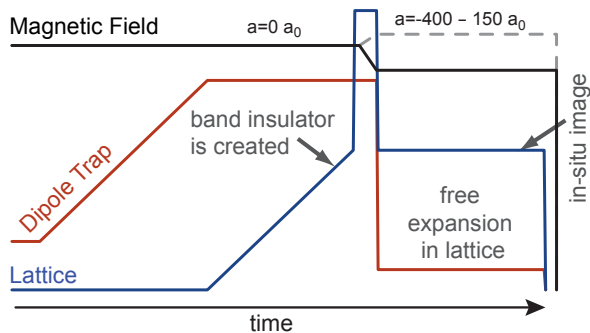


FIG. 7. Experimental Sequence. Starting with a degenerate Fermi gas in the dipole trap a non-interacting band insulator is created. During a freeze-out period the atoms localize to individual lattice sites and the desired interaction is set without altering the density distribution. Subsequently the harmonic confinement is switched off and the cloud expands in a homogeneous Hubbard model.

different lattice sites and effectively localizes all particles to individual sites [41].

In total, this sequence produces a cloud of localized atoms with a well-known density distribution that is independent of the interaction between the particles. The expansion is initiated by lowering the lattice depth in $200\mu s$ to values between $4E_r$ and $15E_r$ while simultaneously switching off the harmonic confinement. To this means, the strength of the dipole trap is reduced by more than 90%, such that the remaining potential precisely compensates the anticonfinement produced by the lattice beams (see Sec. A 4).

2. Theoretical Analysis: Equilibration, Superfast Diffusion and the Breakdown of Hydrodynamics

The hydrodynamic approach is a powerful method to describe the dynamics of interacting liquids. It can be used in many different situation to model the properties of gases (e.g. for the weather forecast), liquids or plasmas both in the classical and quantum regime. As we will show below, in our system the hydrodynamic approach is essential to understand the properties of the center of the interacting atomic cloud where the dynamics is diffusive. It breaks down, however, in its tails where scattering processes of the diluted quantum gas are rare and the dynamics is ballistic. Surprisingly, there is a strong feedback from the ballistic tails to the diffusive core. This feedback can be traced back to a peculiar type of superfast diffusion.

In the following we will first show that a simple hydrodynamic approach based on a diffusion equation is expected to appropriately describe the dynamics in the center, but not close to the border of the atomic cloud, where densities are very low. Due to the specific form of the nonlinear diffusion equation, we will argue that even in the center of the cloud the properties are strongly in-

fluenced by the ballistic boundary. We will therefore analyze and describe the interplay between the diffusive core and the ballistic tails using a Boltzmann equation.

a. Diffusive Regime

The hydrodynamic approach is mainly based on the fact that scattering processes tend to equilibrate the system locally. This equilibration occurs on a time scale τ_{scatt} , the time between collisions of the particles, which depends on the microscopic details of the scattering processes. Similarly, there is an associated length scale ξ_{scatt} , which can be identified with the typical distance an atom travels between two collisions. If the system now is probed on time and length scales much larger than τ_{scatt} and ξ_{scatt} , the microscopic details of the scattering processes are not important any more and the system is *locally* close to equilibrium. The local equilibrium depends only on a small number of conserved quantities that remain invariant under scattering.

Starting point of our analysis is the Hubbard Hamiltonian

$$H = -J \sum_{\langle i,j \rangle} c_{i\sigma}^\dagger c_{j\sigma} + U \sum_i n_{i\uparrow} n_{i\downarrow} \quad (\text{A1})$$

where $c_{i\sigma}^\dagger$ creates a fermion with spin $\sigma = \uparrow/\downarrow$ on lattice site i and where $n_{i\sigma} = c_{i\sigma}^\dagger c_{i\sigma}$. The first term describes the tunneling with rate J from one site of the square lattice to a neighbouring site, while the on-site interaction of the atoms is described by U .

In this section we use units where $\hbar = 1$ and where the lattice constant $\lambda/2$ is set to 1. This has the advantage that the density per area and the density per lattice site take the same values.

For atoms in an optical lattice, momentum can be transferred to the optical lattice by a combination of particle-particle and Bragg scattering and there remain only three conserved quantities in the Hubbard model: the particle number of each of the two species and the energy. As the local magnetization always vanishes in our setup, the hydrodynamic equations can be formulated in terms of two densities only: The number density $n(\mathbf{r}, t)$ and the energy density $e(\mathbf{r}, t)$. In the following, we combine both quantities into a vector $\mathbf{n} = (n, e)$ for notational convenience. The hydrodynamic equations are simply derived from the continuity equation $\partial_t \mathbf{n} + \nabla \mathbf{j} = 0$. The energy and particle currents \mathbf{j} vanish in thermal equilibrium where $\mathbf{n} = \text{const}$. For smooth variations of \mathbf{n} one can expand the current \mathbf{j} to linear order in $\nabla \mathbf{n}$ to obtain the diffusion equation

$$\partial_t \mathbf{n} = \nabla (\mathbf{D}(\mathbf{n}) \nabla \mathbf{n}) \quad (\text{A2})$$

where \mathbf{D} is a two-by-two matrix, describing the energy- and particle diffusion constants and cross terms which arise as energy gradients induce particle flow and vice versa. $\mathbf{D}(\mathbf{n})$ can only be obtained from a microscopic

calculation (see below). For the following discussion it will be essential that for low densities $D(\mathbf{n}) \propto 1/n$, as the scattering rate is proportional to the number of scattering partners (see Sec. A 2 c).

Note that, in one dimension, the hydrodynamic approach cannot be used for the Hubbard model (Eq. A1), since there exists an infinite number of further conservation laws that strongly restrict the possibilities for equilibration.

The diffusion equation (Eq. A2) is valid under the condition that the scattering rates are large compared to the expansion rate $1/\tau_{\text{exp}}$. A quantitative version of this condition can be obtained by linearizing the Boltzmann equation, see Sec. A 2 c, around the local equilibrium solution $f_{\mathbf{q}} \approx f_{\mathbf{q}}^0(\mathbf{n}) + \delta f_{\mathbf{q}}$ with $\delta f_{\mathbf{q}} \propto \tau_{\text{scatt}}$. To leading order in τ_{scatt} one obtains the diffusion equation for \mathbf{n} . By comparing the subleading correction to the current to the leading terms, one obtains the condition

$$\frac{1}{\tau_{\text{scatt}}} \gg \frac{1}{\tau_{\text{exp}}} \approx \frac{|\nabla(\mathbf{D}(\nabla(\mathbf{D}\nabla\mathbf{n})))|}{|\mathbf{D}\nabla\mathbf{n}|} \quad (\text{A3})$$

for the validity of the diffusion equation (Eq. A2). Approximating gradients by the inverse radius of the cloud, $1/R \sim 1/N^{1/3}$, and using $D \approx v^2\tau_{\text{scatt}}$ where $v \sim J$ is a typical velocity, N the total number of particles in the experiment, and J the hopping rate, one obtains that the diffusion equation is valid for

$$\frac{1}{\tau_{\text{scatt}}} \gg \frac{J}{N^{1/3}} \quad (\text{A4})$$

$$n \gg \frac{J^2}{U^2 N^{1/3}} \quad (\text{A5})$$

The second equation is valid for small interactions U only and makes use of the low density approximation $1/\tau_{\text{scatt}} \sim nU^2/J$, see Sec. A 2 c.

An alternative, less rigorous approach to estimate the validity range of the diffusion equation assumes it to be valid as long as the currents $j_{\text{ball}} \approx vn$ for a ballistically expanding cloud are much larger than those obtained from the diffusion equation.

$$j_{\text{diff}} = |D(n)\nabla n| \ll j_{\text{ball}} \approx vn \quad (\text{A6})$$

This results in

$$\frac{1}{\tau_{\text{scatt}}} \gg v \frac{|\nabla n|}{n}, \quad (\text{A7})$$

consistent with Eq. A3 and Eq. A4.

In the thermodynamic limit (defined as usual by $N \rightarrow \infty$ while scaling the initial strength of parabolic confining potentials with $1/N^{2/3}$) the diffusion equation appears to be valid for the whole cloud according to Eq. A5. In the experimental case of 10^5 particles and moderate interactions it should be possible to describe almost all atoms by the diffusion equation Eq. A2. Surprisingly, this conclusion turns out to be incorrect, as can already be seen by analyzing the solutions of the diffusion equation.

b. Breakdown of Hydrodynamics

According to Eq. A3 and the estimate Eq. A5, the diffusion equation is not valid in the tails of the cloud where, due to an extremely small scattering probability, a crossover to ballistic motion is expected. It is, nevertheless, very instructive to study the properties of the diffusion equation Eq. A2, since, as discussed above, the largest part of the cloud remains diffusive. Here we are mainly interested in the low-density regime, where $D(n) \propto 1/n$, since we want to analyze the breakdown of diffusion in the tails. Heat currents are negligibly small for our experiment. Also the dependence of the diffusion constant on energy can be neglected as the local temperatures are always much larger than the bandwidth, $|T/J| \gg 1$, as we have checked numerically. Therefore, we focus on the simple diffusion equation

$$\partial_t n(\mathbf{r}, t) = \nabla \cdot \left(\frac{1}{n(\mathbf{r}, t)^\delta} \nabla n(\mathbf{r}, t) \right) \quad (\text{A8})$$

with $\delta = 1$ in the experiment. A prefactor parameterizing the strength of interactions can be absorbed in a rescaled time variable.

For $\delta > 0$, Eq. A8 is often called fast diffusion equation, for $\delta \geq 1$ superfast diffusion equation [31], and for $\delta = 1$ also the name logarithmic diffusion is used as $\nabla \log n = \frac{1}{n} \nabla n$.

Nonlinear diffusion equations of the form of Eq. A8 are investigated intensively in the mathematical literature, for a review see [31]. Also in physics [42–46] diffusion laws with $\delta = 1$ have been discussed in a small number of publications to describe e.g. the effect of magnetic mirroring in plasmas [44], the kinetics of ion exchange [45], or the spreading of liquid drops on solids in a regime dominated by van-der-Waals forces [46]. A clear picture on how singular hydrodynamic equations and the associated unphysical results have to be regularized and interpreted appears to be missing both in the physical and the mathematical literature. Good examples for the associated theoretical and experimental challenges can, for example, be found in the literature on the dynamics of liquid drops on surfaces. There, mesoscopic precursor films and single-molecular layers apparently play an important role for the regularization of hydrodynamic singularities but their influence on the dynamics remains unclear [47].

Here we will describe some of the basic results relevant for our discussion, mainly based on a review by Vazquez [31]. A lot of insight into the solutions of fast diffusion equations can be obtained by studying simple scaling solutions (the celebrated Barenblatt solutions [48]) of the form

$$n(\mathbf{r}, t) = \frac{1}{t^{d\alpha}} f(r/t^\alpha) \quad (\text{A9})$$

Inserting this ansatz into Eq. A8 one finds in d dimensions

$$\alpha = \frac{1}{2 - d\delta} = \frac{1}{2 - d} \quad (\delta = 1) \quad (\text{A10})$$

indicating that for $d = 3$ no such scaling solution exists while $d = 2$ constitutes the marginal case.

It is also instructive to check the conservation of the total number of particles by integrating the diffusion equation Eq. A8 from $r = 0$ to $r = r_{\max} \rightarrow \infty$:

$$\partial_t N \propto \frac{r^{d-1}}{n^\delta} n'(r) \Big|_{r=r_{\max}} \quad (\text{A11})$$

One immediately realizes that the surface term does not vanish in general, when $n \rightarrow 0$ at the edge of the cloud: particles are lost at $r = \infty$. The importance of the boundary term obviously depends both on δ and d . For our case, $\delta = 1$, a vanishing surface term ($d \ln n / dr < -c/r^{d-1}$ for all $c > 0$) is only possible for $d < 2$ when $\int 1/r^{d-1}$ diverges. A loss of particles is therefore unavoidable for $d \geq 2$, $\delta = 1$.

This implies several quite dramatic consequences which have been worked out in the mathematical literature [31, 32, 49]. As a first surprising result, for a given initial condition $n(r, t = 0)$ with $n(r \rightarrow \infty, 0) = 0$, the diffusion equation Eq. A8 does *not even* have a unique solution for $\delta = 1$! Due to the finite surface contribution one can specify an arbitrary time-dependent current at infinity. For $d = 1$, $\delta = 1$ (or, more precisely, $d < 2$) it is, however, possible to find solutions with a conserved number of particles, e.g. $n(r, t) = 2t/(r^2 + (vt)^2)$ with arbitrary velocity v , consistent with $\alpha = 1$ obtained from Eq. A10. In $d = 3$, in contrast, α is negative indicating the nonexistence of a scaling solution. Indeed, it has been shown [31, 49] that for arbitrary initial conditions with $n(r \rightarrow \infty, 0) = 0$ a solution of the diffusion equation does not exist for $\delta = 1$: all particles reach $r = \infty$ in an infinitesimally short time. The situation is most interesting in two dimensions ($d = 2$), where $\alpha \rightarrow \infty$ according to Eq. A10. This case can easily be analyzed for radially symmetric initial conditions by rewriting $n(r, t) = \tilde{n}(\ln(r), t)/r^2$. For $\delta = 1$ one finds $\tilde{n}(u, t)$ to follow the one-dimensional fast diffusion equation with $\delta = 1$. The total number of particles is *not* conserved but instead drops in time,

$$\partial_t N = -4\pi + 2\pi \lim_{u \rightarrow \infty} \frac{\tilde{n}'(u)}{\tilde{n}(u)} \leq -4\pi \lim_{n \rightarrow 0} [nD(n)] \quad (\text{A12})$$

where we have recovered the correct prefactor in the last term. Interestingly, there is a universal *minimal* loss rate which is *independent* of the size and shape of the cloud [31, 32]. This is due to $\tilde{n}'(u \rightarrow \infty) < 0$, because $n(r, t)$ has to decay faster than $1/r^2$ to obtain a finite particle number $2\pi \int n(r, t) r dr$. The minimal loss rate can, for example, be obtained by solving the diffusion equation for an initial condition $n_\epsilon(r, t = 0) = n_0(r) + \epsilon$ with $n_0(r \rightarrow \infty) = 0$. For finite ϵ the particle number is conserved as $D(n)$ is bounded from above. The limit $\lim_{\epsilon \rightarrow 0} n_\epsilon(r, t)$, however, describes a solution where the minimal loss rate 4π is realized [31]. After a finite time t_{\max} proportional to the total number of particles in the two-dimensional sheet, $t_{\max} \sim U^2/JN_{2d}$, all particles have disappeared.

The diffusion equation predicts them all to have reached $r = \infty$.

In addition, the factor 4π exhibits a direct geometrical interpretation using the relation to the Ricci flow discussed in the main text: For the two-dimensional metric $g_{ij} = n\delta_{ij}$ the total particle number $\int n = \int \sqrt{|\det g|}$ is given by the area of the manifold M , and the particle loss rate from a Ricci flow is given by an integral over the curvature K , $\partial_t N = -2 \int_M K$. For a compact manifold without boundaries, the integral over the curvature, $\int_M K$, is completely fixed by topology. According to the Gauss-Bonnet theorem it is given by 2π times the Euler characteristic, which is 1 in our case, leading to the rate -4π . The extra surface term in Eq. A12 also has a similar interpretation in terms of an integral over the geodesic curvature over the boundary of the manifold.

The mapping for the two-dimensional to the one-dimensional problem also shows that the exponent $\alpha = \infty$ obtained from Eq. A10 for $\delta = 1, d = 2$ can be interpreted as an exponentially fast growth of the cloud, $r \sim \exp(vt)$.

Obviously, the results obtained from the analysis of the diffusion equation are “unphysical” in the sense that in reality there is no particle loss and the cloud cannot expand faster than ballistically in the long-time limit. Nevertheless, the analysis of the diffusion equation shows that there is an unexpected feedback mechanism between diffusive and ballistic regime: The sensitivity of the diffusion equation to boundary conditions clearly shows that the ballistic tails also control the dynamics of the diffusive core. In three dimensions the diffusive core is literally held together by the ballistic tails as the diffusion equation alone would predict that all particles vanish in an infinitesimally short time. Similarly, in the two-dimensional case, where the diffusion equation predicts a universal loss rate of particles at infinity, the crossover from diffusive to ballistic behaviour will affect both regimes.

From a more general point of view, the experimentally realized case, $d = 2, \delta = 1$ constitutes a multicritical point: For $\delta = 1, d = 2$ represents the critical dimension, because particle loss is unavoidable for all $d \geq 2$, as shown above. But also in higher dimensions $\delta = 1$ defines a special point, as can already be seen by using, e.g., an exponential density profile $n \sim e^{-cr}$ in Eq. A12, which yields a diverging (vanishing) particle loss for $\delta > 1$ ($\delta < 1$). Indeed, for $\delta \geq 1$ and $d > 2$ all particles vanish instantaneously at infinity, while for $1 > \delta > 2/d$ solutions exist for finite time intervals [31]. It is therefore both experimentally and theoretically an interesting goal for the future to investigate the interplay of ballistic and diffusive motion for $d = 3, \delta = 1$.

c. Boltzmann equation

In the preceding section we have shown that the feedback from the ballistic tails on the diffusive core of the

atomic cloud controls its expansion. Consequently, an appropriate theoretical description requires a model that can describe both the diffusive and the ballistic regime as well as the crossover between the two. These requirements are met by the Boltzmann equation. A full solution of the space-and time-dependent Boltzmann equation is, however, numerically very demanding. We therefore use a simplified version, which is constructed to be exact both in the diffusive and the ballistic regime and is able to provide a decent qualitative (but not quantitative) description of the crossover regime: We employ a version of the relaxation time approximation that conserves both energy and momentum. Boltzmann equations [50] describe the evolution of the quasiclassical momentum distribution $f_{\mathbf{q}}(\mathbf{r}, t)$ as a function of position and time. Here, the equation is given by

$$\partial_t f_{\mathbf{q}} + \mathbf{v}_{\mathbf{q}} \nabla_{\mathbf{r}} f_{\mathbf{q}} + \mathbf{F}(\mathbf{r}) \nabla_{\mathbf{q}} f_{\mathbf{q}} = -\frac{1}{\tau(\mathbf{n})} (f_{\mathbf{q}} - f_{\mathbf{q}}^0(\mathbf{n})) \quad (\text{A13})$$

where $\mathbf{v}_{\mathbf{q}} = \nabla_{\mathbf{q}} \epsilon_{\mathbf{q}}$ denotes the velocity of the particles and $\mathbf{F}(\mathbf{r})$ describes a force term arising from the interaction of the atoms. For the initial condition we take into account that coherences between neighboring sites are efficiently destroyed during the preparation of the initial state, as described in Sec. A 1. Therefore we use $f_{\mathbf{q}}(\mathbf{r}, t=0) = n(\mathbf{r})$ where $n(\mathbf{r})$ is the density distribution of non-interacting fermions with an entropy per particle of $1.141 k_B$. This entropy corresponds to an initial temperature of $T/T_F \approx 0.125$ in the harmonic trap, which is compatible with the experiment. In the force term, we use the Hartree approximation, $F = -U \nabla n$, where n is the density per spin, but our numerical results show that this term is relatively small. In order to obtain the correct hydrodynamics, the collision term on the right-hand side of Eq. A13 needs to conserve both particle number and energy, and to correctly describe the relaxation towards equilibrium. This is achieved by setting

$$f_{\mathbf{q}}^0(\mathbf{n}) = 1/(\exp[(\epsilon_{\mathbf{q}} - \mu(\mathbf{r}, t))/k_B T(\mathbf{r}, t)] + 1) \quad (\text{A14})$$

where $\mu(\mathbf{r}, t)$ and $T(\mathbf{r}, t)$ are chosen such that both $\sum_{\mathbf{q}} f_{\mathbf{q}} - f_{\mathbf{q}}^0(\mathbf{n}) = 0$ and $\sum_{\mathbf{q}} \epsilon_{\mathbf{q}} (f_{\mathbf{q}} - f_{\mathbf{q}}^0(\mathbf{n})) = 0$. The effective temperatures $T(\mathbf{r})$ obtained from this procedure are, for our initial conditions, at least an order of magnitude larger than the bandwidth. This implies that energy conservation and the diffusion of energy only play a minor role in the experiment, as we checked numerically.

The effective scattering rate $1/\tau(\mathbf{n})$ should be chosen such that the correct diffusion constant $D(\mathbf{n})$ is obtained. Unfortunately, we are not aware of any numerical or analytical method to calculate $D(\mathbf{n}) = \tau(\mathbf{n}) \langle \mathbf{v}_{\mathbf{q}}^2 \rangle / d$ for the two-dimensional Hubbard model, even in the limit $T \rightarrow \infty$, where all thermodynamic properties are exactly known. Note that, for example, dynamical mean field theory, which successfully describes thermodynamic properties [6], should not be used to calculate transport properties quantitatively, as it neglects vertex corrections that are quantitatively important even for $T \rightarrow \infty$.

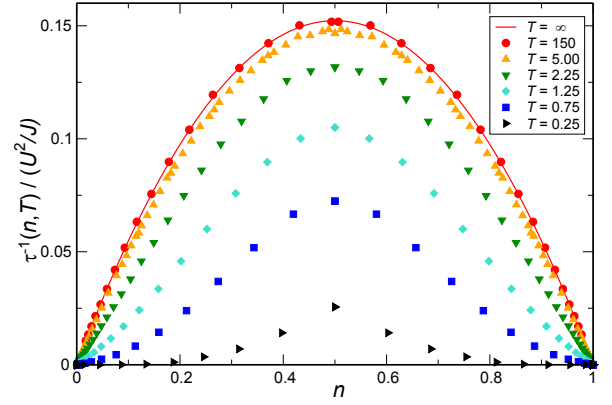


FIG. 8. Transport scattering rates as a function of density for different temperatures. Note that the transport scattering rate (in contrast to the single-particle scattering rate) becomes exponentially small in the low-density, low-temperature regime where Umklapp scattering is suppressed.

We therefore calculate the diffusion constant perturbatively to leading order in the interaction. This can be done by computing the conductivity σ from the translationally invariant Boltzmann equation [50], using the full collision term with golden-rule transition rates. Subsequently, one can obtain $D(\mathbf{n})$ and $\tau(\mathbf{n})$ from the Einstein relation $D = \sigma \partial \mu / \partial n$.

In order to avoid the solution of a complicated integral equation, we employ a variational solution of the Boltzmann equation (see [50] for details) using $f_{\mathbf{q}} = f_{\mathbf{q}}^0 - \partial f_{\mathbf{q}}^0 / \partial \epsilon_{\mathbf{q}} \sum_i \alpha_i c_{\mathbf{q}}^{(i)}$ with four variational parameters α_i , and $c_{\mathbf{q}}^{(1)} = v_{\mathbf{q}}^x$, $c_{\mathbf{q}}^{(2)} = \epsilon_{\mathbf{q}} v_{\mathbf{q}}^x$, $c_{\mathbf{q}}^{(3)} = q_x$, $c_{\mathbf{q}}^{(4)} = (\pi/a - q_x) \bmod 2\pi/a$. Here $c^{(1)}$ and $c^{(2)}$ are chosen to enable the calculation of both thermal and charge diffusion constant as well as the cross terms. The remaining terms, $c^{(3)}$ and $c^{(4)}$, on the other hand, are essential to correctly describe the low temperature limit: For a low density of particles or holes, the conductivity, and therefore the diffusion constant, grows exponentially for low T due to an exponential suppression of Umklapp scattering processes [50]. Since we determine $1/\tau(\mathbf{n})$ such that we recover the correct diffusion constant, this effect is fully included. Note that it is not captured by a more conventional version of the relaxation time approximation [50], which neglects vertex correction and identifies $1/\tau(\mathbf{n})$ with a single-particle relaxation rate instead of a transport scattering rate. Although the variational approach only gives a lower bound for the diffusion constant, we expect it to be accurate within a few percent for small interactions, as we have checked by reducing the number of variational parameters. The density dependence of the resulting scattering rate is shown in Fig. 8 for various temperatures. For $E = 0$ or, equivalently, $T \rightarrow \infty$ we obtain $1/\tau(n, E=0) \approx 0.609 n(1-n)U^2/J$. To solve the resulting Boltzmann equation (Eq. A13), a simple Runge-Kutta integration is used, discretizing both the position and momentum variable.

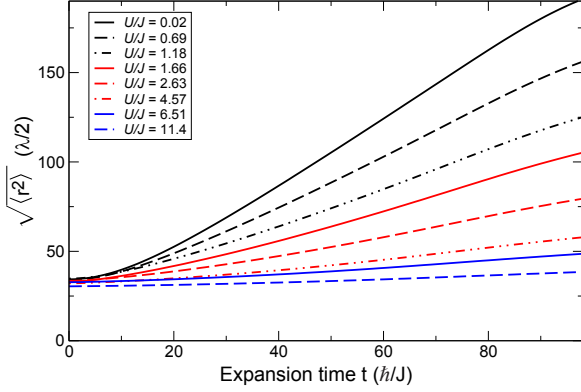


FIG. 9. Cloud size $\sqrt{\langle r^2 \rangle}$, obtained from a simulation of the Boltzmann equation, as a function of expansion time for various interaction strengths. The initial conditions are chosen to match the experimental parameters.

For all quantitative comparisons with the experimental results we also take into account the necessity to average over a stack of independent two-dimensional systems with different atom numbers. This averaging, however, changes the result only slightly since the main contributions arise from the central layers.

d. Interplay of Diffusive and Ballistic Regime

The analysis of the diffusion equation reveals that, in order to appropriately describe the diffusive core of the atomic cloud, one has to include the effect of the ballistic outer regions as well. As the Boltzmann equation describes both regimes and their crossover, it can be used to determine the characteristics of their mutual influence.

Both in the experiment and in the simulation the diffusive and ballistic parts of the atomic cloud can easily be distinguished. The diffusion equation is rotationally invariant, while, in contrast, the cloud becomes quadratic in the ballistic regime due to the square symmetry of both dispersion and Brillouin zone, see Fig. 1 and 6 of the main text. A direct comparison of the density profiles obtained in the simulations and in our experiment demonstrates a very good agreement on all qualitative features. Using scattering rates that were obtained to leading order in perturbation theory, a full quantitative agreement could not be reached. This is discussed in detail in Sec. A 2 e below.

Diffusive and ballistic regimes couple to each other in at least two ways. On the one hand, the diffusive core of the cloud “feeds” the ballistic tails: the diffusive dynamics determines how many particles emerge in the low-density tails of the atomic cloud. On the other hand, the diffusive center is held together by the ballistic tails of the cloud, since the cloud would expand much more rapidly within the diffusion approximation alone. One way of perceiving the interplay of the two regimes is to

study different definitions of the radius of the cloud. Fig. 6 of the main text shows that the mean-square displacement $\langle r^2 \rangle$ is mainly determined by the ballistic tails of the cloud. In contrast, for not too weak interactions, the core width (half width at half maximum HWHM) lies in the diffusive core of the cloud. As the diffusive core melts and loses particles to the ballistic outer regions it is therefore not surprising that, for large interactions, the core width *shrinks* as a function of time (both in theory and experiments). $\langle r^2 \rangle$, on the other hand, always grows (see Fig. 9).

An interesting question concerns the long-time asymptote of the cloud radius: Does it show power-law behaviour $r \sim t^\alpha$ in at least some regime? A related question is whether the universal loss rate of particles obtained from the hydrodynamic theory in $d = 2$ has any direct consequences.

To study these questions, it is useful to first investigate the behaviour of the ballistic part of the cloud. The diffusive core can be viewed as a source of ballistic particles. In order to obtain a qualitative impression of the shape and effective radius of the ballistic part of the atomic cloud, we can use a simple model: At $r = 0$, ballistic particles are created with rate $W(t)$ and momentum distribution $n_{\mathbf{q}}$, which is assumed to be time independent. A ballistic particle created at time t_0 at $\mathbf{r} = 0$ with velocity $\mathbf{v}_{\mathbf{q}}$ can be found at later times t at $\mathbf{r} = \mathbf{v}_{\mathbf{q}}(t - t_0)$. Thus, we obtain the following density distribution of the ballistic atoms:

$$n_{\text{ball}}(\mathbf{r}, t) = \int \frac{d^d q}{(2\pi)^d} n_{\mathbf{q}} \int_0^t dt_0 W(t_0) \delta^d(\mathbf{r} - \mathbf{v}_{\mathbf{q}}(t - t_0)) \quad (\text{A15})$$

More realistically, one can assume that the particles are created at a finite radius r_c , which avoids, e.g., an unphysical logarithmic singularity on the diagonal $x = y$. Since we are mainly interested in the limit $r \gg r_c$, we ignore this effect. As shown in Fig. 6, the mean radius $\sqrt{\langle r^2 \rangle}$ is dominated by the ballistic part of the cloud. Therefore, for a single two-dimensional sheet with N_{2d} atoms per spin, we can estimate

$$\begin{aligned} \langle r^2 \rangle_t - \langle r^2 \rangle_{t=0} &\approx \frac{\int \mathbf{r}^2 n_{\text{ball}}(\mathbf{r}, t) d^2 \mathbf{r}}{N_{2d}} \\ &= \langle \mathbf{v}_{\mathbf{q}}^2 \rangle \frac{\int_0^t W(t_0) (t - t_0)^2 dt_0}{\int_0^\infty W(t_0) dt_0} \end{aligned} \quad (\text{A16})$$

Finally, for $t \rightarrow \infty$, all particles become ballistic, thus $\int_0^\infty W(t_0) dt_0 = N_{2d}$.

Since the diffusion equation predicts the disappearance of particles at infinity with a universal, time-independent rate, we define a time t_{max} such that $W(t) \approx N_{2d}/t_{\text{max}}$ for $t < t_{\text{max}}$ and $W(t) = 0$ for $t > t_{\text{max}}$. This leads to:

$$\langle r^2 \rangle_t - \langle r^2 \rangle_{t=0} \approx \langle \mathbf{v}_{\mathbf{q}}^2 \rangle \begin{cases} t^3/(3t_{\text{max}}) & \text{for } t < t_{\text{max}} \\ t^2 & \text{for } t \gg t_{\text{max}} \end{cases} \quad (\text{A17})$$

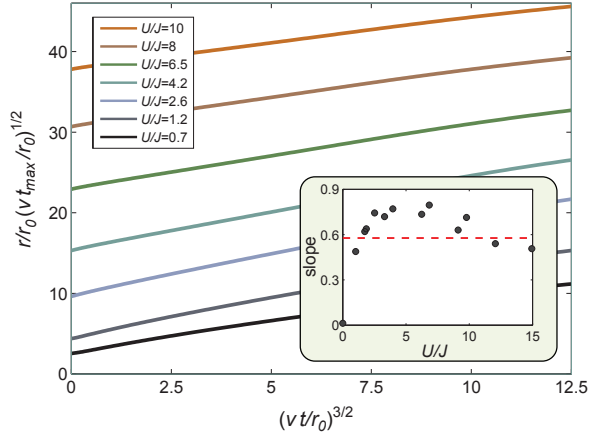


FIG. 10. Cloud size $\sqrt{\langle r^2 \rangle}$ as a function of $t^{3/2}$ (in rescaled units). While the core width (half width at half maximum HWHM) of the atomic cloud measures the radius of the diffusive core, the average $\sqrt{\langle r^2 \rangle}$ is mainly sensitive to the ballistic tails. From the numerical solution of the Boltzmann equation, we find that $\sqrt{\langle r^2 \rangle}$ grows as $t^{3/2}$ for long times, see [30]. Remarkably, the prefactor of the $t^{3/2}$ law (see inset) can be calculated analytically (dashed line) from the universal loss rate of the diffusion equation discussed in Eq. A12. For weak interactions and much longer times, $t \gg t_{\max}$, the whole cloud is ballistic with $\sqrt{\langle r^2 \rangle} \propto t$.

Interestingly, precisely this behaviour is observed in our numerical solution of the Boltzmann equation. In Fig. 10 the size of the cloud, $r = \sqrt{\langle r^2 \rangle}$, scaled by $v t_{\max}$, is plotted as a function of $t^{3/2}$. Here, as before, $v = \sqrt{\langle \mathbf{v}^2 \rangle}$ denotes a typical ballistic velocity. Remarkably, one does not only obtain $r/(v t_{\max}) \sim t^{3/2}$ for $t < t_{\max}$ but also that the prefactor is independent of the interaction strength!

Eq. A12 yields an estimate of the prefactor of the $t^{3/2}$ behaviour

$$t_{\max} \approx N_{2d}/(4\pi \lim_{n \rightarrow 0} [nD(n)]). \quad (\text{A18})$$

This prefactor differs by less than 20% from the one observed in the numerical solution of the Boltzmann equation in the high-density limit, see Fig. 10. A similar behaviour is also found for initial conditions with a much smaller central density, $n \ll 1$, as long as $t < t_{\max}$ (not shown).

Overall, the agreement of the numerical simulations and the simple model (Eq. A17) is rather surprising as the diffusive behaviour is strongly modified by the ballistic outer regions, which prohibit a too fast expansion of the cloud. Here one should note that from the present numerical data we cannot rule out an additional very weak logarithmic dependence of the prefactor on cloud size, interaction strength, or time, which would not be surprising as $d = 2$ is the ‘critical’ dimension of the problem as discussed above.

e. Origin of quantitative discrepancies of theory and experiment

While the numerical results qualitatively reproduce all experimentally observed features, a quantitative comparison shows that the experimentally observed expansion rates of the cloud are consistently larger than the estimates obtained from our numerical results. Note that there are no fitting parameters involved as both the hopping rates and the interaction strengths are known. The error bars in J and U cannot explain the observed discrepancies.

There are several candidates that could explain the discrepancies between theory and experiment: In the non-interacting case, where there are no theoretical uncertainties, the agreement of theory and experiment concerning the size of the cloud is very good and pronounced discrepancies in the shape only occur for large clouds, where residual potentials and inhomogeneities in the hopping rates become important, see Fig. 2 in the main text and Sec. A4 below. Due to the much smaller core widths, however, we do not believe that these effects are important in the interacting case.

A second problem might be the variational estimate for the diffusion constant, which gives only a lower bound for D . While the experimentally observed cloud sizes are indeed larger than the theoretical predictions, we do not believe that errors due to the bound are able to explain the discrepancy (see discussion in section A2c above).

A more serious problem is the use of perturbative formulas for the diffusion constant, which are only valid for weak interactions, formally $U \ll 4J$. A quantitative discrepancy for large interactions is therefore not surprising. We were, however, not able to identify a clear trend whether the theory fits better for weaker interactions. Consequently, this argument does not give a convincing explanation either.

In our opinion, the most likely origin of the observed discrepancy lies in a breakdown of the relaxation time approximation in the crossover regime between the diffusive core of the cloud and its ballistic tails. Deep in the ballistic regime, the scattering rate is negligibly small. Similarly, deep in the diffusive regime, the relaxation time approximation should be valid: To good approximation, a local equilibrium is established and we have determined $1/\tau(\mathbf{n})$ in such a way that the correct diffusion constants are reproduced. Yet in the crossover regime, the distribution functions $f_{\mathbf{q}}$ are far from equilibrium. Here, the relaxation time approximation should result in an error of order one. While this crossover regime only affects a small portion of the cloud, we know from our analysis of the diffusion equation in Sec. A2b that boundary conditions are very important for diffusion equations. Consequently, the crossover regime will have a strong influence even on the core width of the cloud, which, for moderate interactions, is determined from the portion of the cloud where the diffusion equation should be valid.

3. Dynamical $U \rightarrow -U$ symmetry of the Hubbard model

In the following we address the observed dynamical symmetry between repulsive and attractive interactions in the fermionic Hubbard model. As discussed in the main text, this symmetry arises from the high symmetry of the tight binding dispersion $E_{\mathbf{q}} = -2J \sum_i \cos(q_i \frac{\lambda}{2})$. In order to understand this, let us consider a single momentum component, say $\hbar q_x$, whose dispersion and group velocity distribution are plotted in Fig. 11:

The maximum group velocity $v_{\max} = \max(\frac{1}{\hbar} \frac{\partial E_q}{\partial q_x})$ corresponds to the state with quasi-momentum $\hbar q_x = \hbar\pi/\lambda$ and energy $E_q = 0$, while states with finite energy, either positive or negative, have a smaller velocity. Using this group velocity distribution, the symmetry of expansion under the change of the sign of U can intuitively be understood as follows: Attractive interactions reduce the kinetic energy of the particles, which slows them down. Repulsive interactions increase their kinetic energy which, surprisingly, slows them down as well.

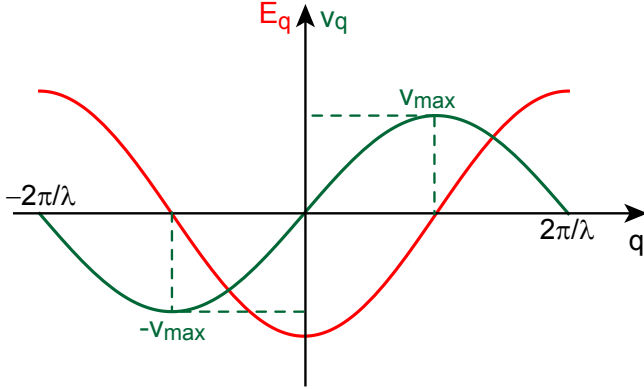


FIG. 11. Single particle energy E_q and corresponding velocity v_q in the Hubbard model.

In the following we will turn this qualitative argument into a rigorous theorem revealing this counter-intuitive dynamical symmetry of the Hubbard model:

We consider a coherent dynamical evolution arising from two Hubbard-type Hamiltonians that differ only in the sign of the interaction term:

$$\mathcal{H}_{\pm} = -J \sum_{\langle ij \rangle \sigma} c_{i\sigma}^{\dagger} c_{j\sigma} \pm U \sum_i n_{i\uparrow} n_{i\downarrow} \quad (\text{A19})$$

In addition, we define two symmetry operations: The time reversal operator R_t and the π -boost operator B_Q , which translates all quasi-momenta by $Q = (\pi, \pi, \pi) \times \frac{\lambda}{2}$. Applying the time reversal operator turns the wavefunction into its complex conjugate [51] or, equivalently, modifies the time evolution operator:

$$R_t e^{-i\mathcal{H}t} R_t^{\dagger} = e^{i\mathcal{H}t} \quad (\text{A20})$$

The action of the π -boost operator is given in second

quantized notations by

$$B_Q c_p B_Q = c_{p+Q} \quad (\text{A21})$$

or, in real space:

$$B_Q c_j B_Q = e^{iQr_j} c_j \quad (\text{A22})$$

We now formulate the following general theorem:

If both the initial state $|\Psi_0\rangle$ and the experimentally measured quantity O are invariant under both time reversal and π -boost, the observed time evolutions

$$\langle O(t) \rangle_{\pm} = \langle \Psi_0 | e^{i\mathcal{H}_{\pm}t} O e^{-i\mathcal{H}_{\pm}t} | \Psi_0 \rangle \quad (\text{A23})$$

are identical: $\langle O(t) \rangle_{+} = \langle O(t) \rangle_{-}$.

In order to verify the last statement we first observe that

$$\begin{aligned} \langle O(t) \rangle_{+} &= \langle \Psi_0 | R_t^{\dagger} R_t e^{i\mathcal{H}_{+}t} R_t^{\dagger} R_t O R_t^{\dagger} R_t e^{-i\mathcal{H}_{+}t} R_t^{\dagger} R_t | \Psi_0 \rangle \\ &= \langle \Psi_0 | e^{-i\mathcal{H}_{+}t} O e^{i\mathcal{H}_{+}t} | \Psi_0 \rangle \end{aligned} \quad (\text{A24})$$

The last equation follows from the definition of time invariance, $R_t |\Psi_0\rangle = |\Psi_0\rangle$ and $R_t O R_t^{\dagger} = O$, and from the unitarity property $R_t^{\dagger} R_t = 1$. Note that equation (A24) corresponds to the symmetry of time evolutions for $\mathcal{H} \rightarrow -\mathcal{H}$, which has been discussed previously in References [52, 53]. From the definition of the π -boost we get

$$B_Q \mathcal{H}_{\pm} B_Q = -\mathcal{H}_{\mp} \quad (\text{A25})$$

and can continue equation (A24):

$$\langle O(t) \rangle_{+} = \langle \Psi_0 | B_Q^2 e^{-i\mathcal{H}_{+}t} B_Q^2 O B_Q^2 e^{i\mathcal{H}_{+}t} B_Q^2 | \Psi_0 \rangle = \langle O(t) \rangle_{-}$$

In the last equation we used the assumed π -boost invariance of the observable $B_Q O B_Q = O$ and the initial state $B_Q |\Psi_0\rangle = |\Psi_0\rangle$, as well as unitarity $B_Q^2 = 1$.

In the experiment, we measure the density distribution $n(r_j) = \sum_{\sigma} c_{j\sigma}^{\dagger} c_{j\sigma}$ and the initial state consists of atoms that are completely localized to individual lattice sites (see Sec. A1). Because both the initial state and the measured operator are invariant under time-reversal and π -boost, we are guaranteed to find the $U \rightarrow -U$ symmetry in the dynamics for all interaction strengths.

It is interesting to note that the bi-partite character of the lattice was crucial to our proof of the symmetry. Thus we do not expect to find this symmetry in lattices without the bi-partite structure, such as a triangular lattice.

4. Non-Interacting atoms: Canceling the harmonic confinement

Figure 12 shows the cloud sizes $R_G(t)$ of an expanding non-interacting cloud in an $8 E_r$ deep quasi 2D lattice as a function of the dipole laser power during the expansion. The red line denotes a fit with the expected dynamics (Eq. 3) to the first 20 ms. While the initial

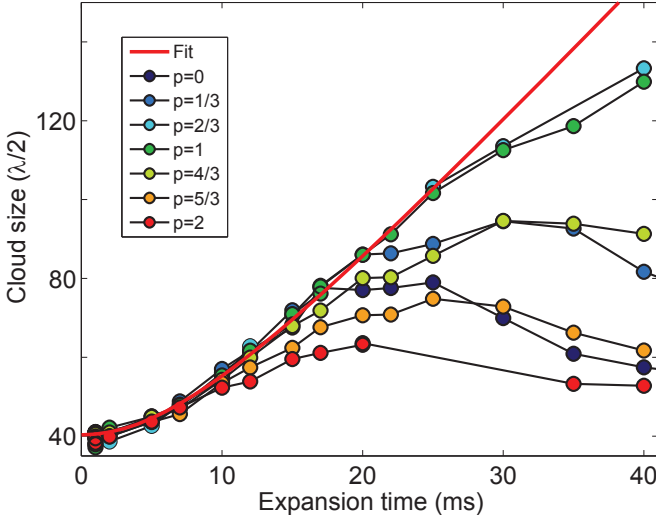


FIG. 12. Expansion of non-interacting atoms as a function of dipole beam power p (a.u.) in an $8E_r$ lattice.

expansion velocity depends only slightly on the residual confinement, it completely dominates the size after long expansion times.

The largest cloud sizes are reached if the confinement created by the dipole trap precisely compensates the anticonfinement due to the lattice. This situation corresponds to dipole powers between $p = 2/3$ and $p = 1$ in Fig. 12. Both an over- and an under-compensation lead to deviations from the expected ballistic behaviour and limit the cloud size by either classical reflections or Bragg reflections of the expanding atoms.

In the well-compensated case the leading correction to the homogeneous Hubbard model (Eq. A1) arises from the fact that the hopping rate in any given direction becomes larger when an atom is not any more in the center of the corresponding laser beam. This effect can easily be described quantitatively by modeling the experimental laser profiles. For a distance of 100 lattice constants from the center, the hopping rate increases by about 25%. Figure 13 shows the resulting density profiles in the non-interacting case, which reproduce all features of Fig. 2 of the main text with the exception of the last panel at 80 ms, where additional potentials due to technical imperfections in the alignment and beam shapes of the dipole and lattice beams become important.

In the interacting case the clouds remain much smaller and these effects can completely be neglected.

5. Image processing and fitting

In the non-interacting case the perpendicular cloud size $\sqrt{\langle r^2 \rangle}$ is extracted from in-situ phase-contrast images using a 2D Gaussian fit:

$$G(x, y) = A e^{-\frac{(x-x_c)^2}{2\sigma_x^2} - \frac{(y-y_c)^2}{2\sigma_y^2}} + b \quad (\text{A26})$$

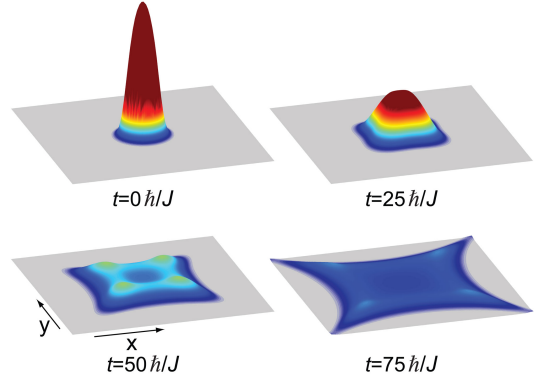


FIG. 13. Simulated column density distribution for the non-interacting expansion including the finite size of the lattice beams.

Here $x_c, y_c, \sigma_x, \sigma_y, A, b$, are free fit parameters and the perpendicular cloud size is given by $\sqrt{\langle r^2 \rangle} = R_G = \sqrt{\sigma_x^2 + \sigma_y^2 - w^2}$, where w denotes the imaging resolution (radius of Airy disc $w < 3\mu\text{m}$) of our imaging setup.

The corresponding single-particle width $R_{sp}(t)$ is calculated by deconvolving $R_G(t)$ with the initial width $R_G(0)$: $R_{sp}(t) = \sqrt{R_G(t)^2 - R_G(0)^2}$. An example of the expanded single-particle width is shown in Fig. 3 in the main text and agrees well with the linear slope expected for a ballistic expansion.

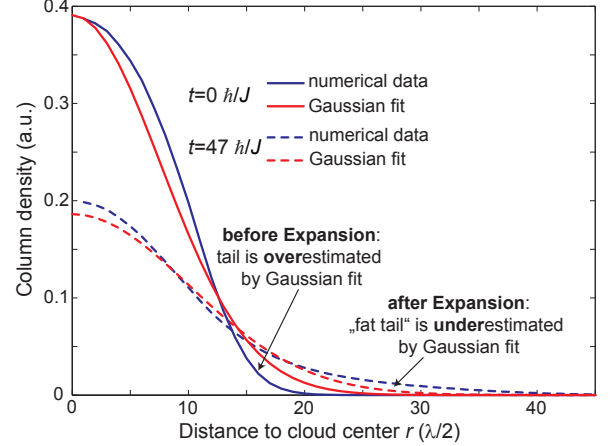


FIG. 14. Numerically calculated density distribution for $U/t = 1.2$ together with Gaussian fits.

In the case of interacting atoms the shape of the cloud changes considerably during the expansion, evolving from a “compact” Fermi-Dirac like shape (Supporting Online Material of Ref. [6]) to a “fat tail” distribution, as illustrated in Fig. 14 using fits to numerically simulated data. This leads to considerable systematic errors in the estimation of $\langle r^2 \rangle$ ($\neq R_G^2$) in the interacting case. In principle, such systematic errors could be avoided by determining $\langle r^2 \rangle$ via direct integration, analogous to the numerical data in Fig. 9. In the experiment, however,

this is hindered by imaging aberrations and the small signal to noise ratio in the extreme dilute limit.

The change in the shape of the cloud is due to the density dependent dynamics in the interacting case: While the expansion remains ballistic in the low density limit, where the mean free path is larger than the distance to the cloud edge, the expansion velocity decreases for higher densities due to the increasing number of collisions. As a consequence, $\langle r^2 \rangle$ will be dominated by the ballistically expanding outermost atoms (see Fig. 6) for long expansion times.

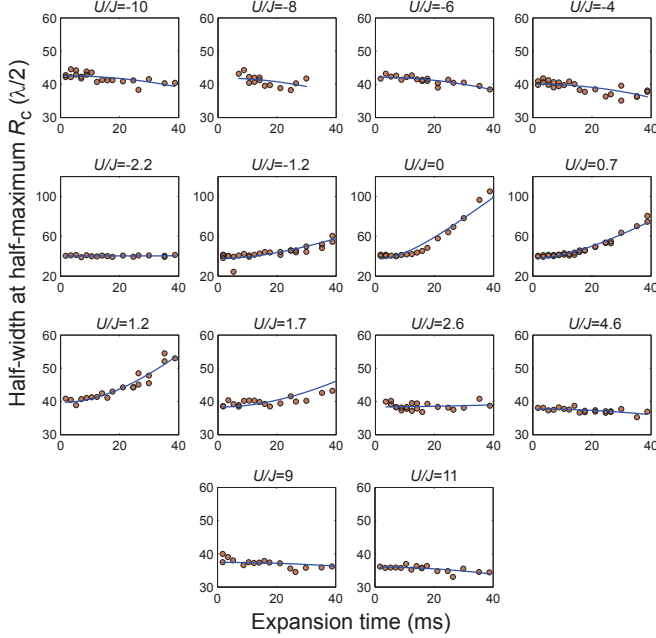


FIG. 15. Core widths R_c as a function of expansion time for various interactions in an $8 E_r$ deep lattice in the 2D case. Blue lines denote the fits used to extract the core expansion velocities (Eq. A27)

In order to focus on the core dynamics we instead use the core width R_c , which denotes the half width at half maximum (HWHM) of the azimuthally averaged column density distribution, where each distribution is individually normalized. This core widths shown in Fig. 15 are fitted by the same fit function as in the non-interacting

case

$$R_c(t) = \sqrt{R_c(0)^2 + v_c^2 t^2} \quad (\text{A27})$$

and the resulting core expansion velocities v_c are shown in Fig. 5 in the main text.

6. Width of Feshbach resonance

The interactions are controlled by use of the well-known Feshbach resonance at $B_0 = 202.1$ G between the two lowest hyperfine states $|F, m_F\rangle = |9/2, -9/2\rangle$ and $|9/2, -7/2\rangle$ [35]. Compared to previous dipole trap experiments, the dynamics in the lattice are much more sensitive to small scattering lengths, since the strongly reduced kinetic energy of atoms in a lattice enhances the role of interactions. The observed pronounced dependence on small interactions (Fig. 5) enabled us to remeasure the zero crossing of the scattering length, which we found to be at $B(a = 0) = 209.1 \pm 0.2$ G. Using the standard parametrization of the (free space) Feshbach resonances

$$a(B) = a_{bg} \left(1 - \frac{w}{B - B_0} \right) \quad (\text{A28})$$

this zero crossing leads to a new width of

$$w = 7.0 \pm 0.2 \text{ G} \quad (\text{A29})$$

compared to the previous dipole trap measurement of $w_{\text{dipole}} = 7.8 \pm 0.6$ G (PhD. Thesis C. Regal, JILA). In addition to the pronounced dependence of the slope, only the expansion at the newly assigned zero crossing matches that of a single component Fermi gas under the same conditions and leads to the square shape expected for non-interacting atoms.

7. Doublon dissolution time

The number of atoms on doubly occupied lattice sites is measured by converting all doublons into molecules. This is achieved by first increasing the lattice depth to $20 E_r$ in $200 \mu\text{s}$, followed by a magnetic field ramp (5 G/ms) over the Feshbach resonance [6]. The resulting doublon numbers are fitted by a simple exponential decay.